

**Electric and magnetic field manipulation and storage of charge-tunable excitons**

J. Simonin and C. R. Proetto

*Centro Atómico Bariloche and Instituto Balseiro, C.P. 8400, San Carlos de Bariloche, Río Negro, Argentina*

M. Pacheco and Z. Barticevic

*Departamento de Física, Universidad Santa María, Casilla 110-V, Valparaíso, Chile*

(Received 23 December 2013; published 7 February 2014)

The excitonic spectrum of radially polarized semiconductor rings has been analyzed theoretically, in the presence of an in-plane electric field and a perpendicular magnetic field. Based on the numerically exact solution, a regime has been found where the exciton behaves as a single carrier or quasiparticle, with an effective and tunable electric charge determined by the ring geometry. A protocol is proposed for the storage of excitons without destroying them, consisting in converting them from “bright” to “dark,” by performing a sequence of well-defined steps. Accurate analytical approximations are provided for each of the exciton regimens found: quasifree, locked, and broken.

DOI: [10.1103/PhysRevB.89.075304](https://doi.org/10.1103/PhysRevB.89.075304)

PACS number(s): 78.67.Bf, 73.21.-b, 73.40.Rw, 78.66.Fd

**I. INTRODUCTION**

Nanoscale semiconductor structures have been the subject of numerous theoretical and experimental investigations in the last few years. The effects of quantum confinement in these nanosystems strongly modify their electronic and optical properties, offering exciting possibilities for technological applications. Among these, a particular class of structures with annular geometry called nanorings is being intensively investigated after the experimental observation of the Aharonov-Bohm effect [1] (ABE) in small metallic rings [2–5]. With the developments in nanofabrication, the formation of different types of semiconductor nanorings is now possible [6]. Most of the experimental work is based on self-assembled nanorings made of InAs quantum dots capped with a thin GaAs layer subjected to a short (but crucial) annealing, but also lithographic techniques have also been used for the fabrication of InGaAs nanorings [7]. The self-assembling of non-III-V semiconductor nanorings of SiGe has been achieved too [8]. The tendency toward enlargement of the semiconductor nanoring family in the nearest future is quite clear by now.

This gives us the exciting opportunity to observe new quantum interference phenomena in magneto-optical experiments [7,9]. Several theoretical papers have reported studies about the influence of the different geometric-confinement parameters and of the presence of impurities on the spectrum in a semiconductor quantum ring in a magnetic field [10–13]. The effects of an external electric field on the Bohm-Aharonov oscillations in the energy spectrum of single carriers in quantum rings have been also reported [14]. Most of the experimental work has been performed on charged excitons in nanorings [7,9,15,16] and a little on neutral excitons in type-II quantum dots [17]. The possibility of observation of the so-called “optical” ABE for neutral excitons has been an interesting and controversial subject in recent years [18–21]. It has been predicted that the polarization of a neutral exciton in a quantum ring may give rise to a magnetic interference effect such that the ground state of the exciton acquires a nonzero angular momentum for increasing magnetic field [22–25]. The finite polarization of an exciton can be realized by asymmetries

in the confinement potentials of the electrons and holes or by means of a uniform electric field applied in the ring plane [26].

This work analyzes the effects induced by an in-plane electric field on the excitonic spectrum of semiconductor quantum rings. We adopt the effective-mass theory and consider radial polarized quantum rings [27] in which the excitonic Hamiltonian is written under the assumptions that the electron and hole coordinates along the ring-axis direction may be “frozen” at the same in-plane value, and that the radial displacements of the electron and hole may be frozen at different radial coordinates. The electron-hole Coulomb attraction is treated rigorously, through numerical diagonalization of the full exciton Hamiltonian in the basis of noninteracting electron-hole pairs. The electric field breaks the azimuthal symmetry and mixes the eigenfunctions with different angular momenta. We write the two-dimensional excitonic wave functions as linear combinations of the eigenfunctions of the orbital total angular momentum operator. We have found before [28] that Aharonov-Bohm oscillations are discernible in the exciton ground-state energy of small rings; this is the weak-interacting kinetic-energy-dominated regime (or extended regime) [29]. In the limit of large rings, the system is driven in the Coulomb-dominated strongly interacting regime (or localized regime), where the exciton is basically a neutral and compact object, with small sensitivity to the magnetic field. In the presence of a radial (in-plane) electric field, which is the case addressed in this work, a new energy scale appears, and the large-size ring limit is dominated by the electric field. This can be understood easily from the way in which the relevant magnitudes scale with ring size ( $\sim R$ ): kinetic energy scales as  $R^{-2}$ , the Coulomb interaction as  $R^{-1}$ , and the electric field as  $R$ . In the localized regime, the electric field destroys the Aharonov-Bohm oscillations of the ground state. In addition to analytical results well inside each one of the different regimens, we present numerical results, mainly related to the electric-field-induced rupture of the exciton bound state. Based on the numerically exact solution, we have identified three different regimens for the exciton, for increasing values of the electric field: (a) quasifree excitons; (b) locked excitons; and (c) electron-hole-pair or broken excitons. We also propose possible protocols for the dynamical

storage of excitons without destroying them, consisting in converting them from “bright” to “dark,” by a suitable combination of electric and magnetic fields. This may have some impact on the context of trapping light for later use.

## II. THE MODEL AND METHOD OF SOLUTION

The effective-mass Hamiltonian for an electron-hole double-nanoring structure, subject to both an external magnetic field perpendicular to the ring plane and an in-plane electric field, can be simplified under some assumptions. In the first place, the electron and hole coordinates along the  $z$  direction may be frozen at the same in-plane value  $z_e = z_h = 0$ . This is consistent with the fact that for all the semiconductor quantum rings produced by today’s semiconductor growth techniques, the confinement along the  $z$  direction (usually given by a compositional barrier between two different closely lattice-matched semiconductors) is much stronger than the in-plane confinement. This gives rise to a strong quantization along  $z$ . In the second place, the radial displacements of the electron and hole may also be frozen at different radial coordinates  $R_e$  and  $R_h$  respectively. This is related to the facts that the effective self-consistent potentials, for the electron and the hole, have in general different radial positions for their respective minima [30,31], and that the quantization in the radial direction is stronger than in the azimuthal direction for both of them. Therefore, the excitonic Hamiltonian is ( $e > 0$ ) [23]

$$H_{\text{exc}}(\theta_e, \theta_h) = H_{\text{exc}}^{(0)}(\theta_e, \theta_h) + U_c(\Delta\theta) + H_F(\theta_e, \theta_h), \quad (1)$$

where

$$H_{\text{exc}}^{(0)}(\theta_e, \theta_h) = \frac{\hbar^2}{2I_e} \left( -i \frac{\partial}{\partial \theta_e} + \frac{\phi_e}{\phi_0} \right)^2 + \frac{\hbar^2}{2I_h} \left( i \frac{\partial}{\partial \theta_h} + \frac{\phi_h}{\phi_0} \right)^2, \quad (2)$$

$$U_c(\Delta\theta) = -\frac{e^2}{\epsilon \sqrt{R_e^2 + R_h^2}} \frac{1}{\sqrt{1 - r \cos(\Delta\theta)}}, \quad (3)$$

and

$$H_F(\theta_e, \theta_h) = -eF(R_e \cos \theta_e - R_h \cos \theta_h). \quad (4)$$

Also, the excitonic eigenfunctions of  $H_{\text{exc}}(\theta_e, \theta_h)$  are denoted as  $\varphi_i(\theta_e, \theta_h)$ , with  $i$  corresponding to the exciton quantum numbers; the corresponding eigenvalues are denoted by  $E_i(B, F)$ . In addition, in the above equations,  $(R_e, \theta_e)$  and  $(R_h, \theta_h)$  are the radial and angular electron and hole polar coordinates, respectively;  $\Delta\theta = \theta_e - \theta_h$ .  $m_e^*$  and  $m_h^*$  are the electron and hole effective masses, and  $I_x = m_x^* R_x^2$ , with  $x = e, h$ , are the moments of inertia.  $\phi_x = \pi R_x^2 B$  are the magnetic fluxes threading the electron and hole rings, and  $\phi_0 = ch/e$  is the flux quantum.  $U_c(\Delta\theta)$  describes the Coulomb attraction between the electron and the hole, with  $\epsilon$  the dielectric constant of the semiconductor ring material, and  $r = 2R_e R_h / (R_e^2 + R_h^2)$ . This parameter  $r$  determines the shape of the Coulomb interaction. For  $r \rightarrow 0$  ( $R_h \gg R_e$ ) the Coulomb potential as a function of  $\Delta\theta$  is nearly flat, while for  $r \rightarrow 1$  ( $R_h \simeq R_e$ ), the potential has a pronounced minimum at  $\Delta\theta = 0$ . For suitable values of  $R_e$  and  $R_h$  it generates a strong excitonic state [28]. Here we study the effects of the in-plane electric field  $F$  on that exciton,

the effect of the electric field being represented by the term  $H_F(\theta_e, \theta_h)$ .

Alternatively, and using the generalized angular “center of mass” (c.m.) coordinate  $\theta_0 = (I_e \theta_e + I_h \theta_h) / I$ ,  $I = I_e + I_h$ , the exciton Hamiltonian of Eq. (1) may be conveniently reexpressed as

$$H_{\text{exc}}(\theta_0, \Delta\theta) = H_{\text{c.m.}}(\theta_0) + H_{\text{int}}(\Delta\theta) + H_F(\theta_0, \Delta\theta), \quad (5)$$

where

$$H_{\text{c.m.}}(\theta_0) = \frac{\hbar^2}{2I} \left( -i \frac{\partial}{\partial \theta_0} + \frac{\phi_{\text{c.m.}}}{\phi_0} \right)^2, \quad (6)$$

$$H_{\text{int}}(\Delta\theta) = \frac{\hbar^2}{2I_{\text{int}}} \left( -i \frac{\partial}{\partial (\Delta\theta)} + \frac{\phi_{\text{int}}}{\phi_0} \right)^2 + U_c(\Delta\theta), \quad (7)$$

and

$$H_F(\theta_0, \Delta\theta) = eF \left\{ \cos \theta_0 \left[ R_h \cos \left( \frac{I_e \Delta\theta}{I} \right) - R_e \cos \left( \frac{I_h \Delta\theta}{I} \right) \right] + \sin \theta_0 \left[ R_e \sin \left( \frac{I_h \Delta\theta}{I} \right) + R_h \sin \left( \frac{I_e \Delta\theta}{I} \right) \right] \right\}. \quad (8)$$

Here,  $\phi_{\text{c.m.}} = \pi B(R_e^2 - R_h^2)$ ,  $I_{\text{int}} = I_e I_h / I$ , and  $\phi_{\text{int}} = \pi I_{\text{int}} B / \mu$ , with  $\mu = m_e^* m_h^* / (m_e^* + m_h^*)$ . In the absence of any electric field, the contribution  $H_F(\theta_0, \Delta\theta)$  vanishes, and an exact decoupling of the translational ( $\theta_0$ ) and relative ( $\Delta\theta$ ) coordinates is achieved. In that case, the exciton wave function may be rigorously expressed as the product of a c.m. and relative coordinate wave function, eigenfunctions of  $H_{\text{c.m.}}(\theta_0)$  and  $H_{\text{int}}(\Delta\theta)$ , respectively. Each eigenfunction can be characterized with a single quantum number: the total angular quantum number  $L = l_e + l_h$  for the eigenfunctions of  $H_{\text{c.m.}}(\theta_0)$ , and an internal quantum number  $n$  for the eigenfunctions of  $H_{\text{int}}(\Delta\theta)$ . Since the zero-electric-field Hamiltonian is the sum of two uncoupled terms, the eigenvalues are given by

$$E_{L,n}(B) = \frac{\hbar^2}{2I} \left( L + \frac{\phi_{\text{c.m.}}}{\phi_0} \right)^2 + \varepsilon_{L,n}(B), \quad (9)$$

with  $\varepsilon_{L,n}(B)$  being the eigenvalues of  $H_{\text{int}}(\Delta\theta)$ . If the electric field is not zero,  $H_F(\theta_0, \Delta\theta)$  couples the c.m. and relative coordinates, and the  $(L, n)$  quantum numbers are replaced by a single one “ $i$ ”, which just distinguishes the different solutions of Eq. (5). Even in that case, however, Eq. (5) is a useful starting point for the analysis of the numerical results to be show below, particularly in the weak electric-field limit.

We have used the following numerical strategies for obtaining numerically exact results: [28] full diagonalization and/or recursive Lanczos method, in the non-interacting electron-hole pairs basis generated by the eigenstates of  $H_{\text{exc}}^{(0)}(\theta_e, \theta_h)$ ,

$$\psi_{l_e, l_h}^0(\theta_e, \theta_h) = \frac{1}{(2\pi)} e^{il_e \theta_e} e^{il_h \theta_h}, \quad (10)$$

with  $\theta_x = [0, 2\pi]$ , and with energy

$$E_{l_e, l_h}^0(B) = \frac{\hbar^2}{2I_e}(l_e + \phi_e)^2 + \frac{\hbar^2}{2I_h}(l_h - \phi_h)^2. \quad (11)$$

Here,  $l_e$  and  $l_h (= 0, \pm 1, \pm 2, \dots)$  are the electron and hole angular momentum quantum numbers, respectively.

In brief, while the exciton Hamiltonian as given in Eq. (1) is useful for introducing the model and is the form we use for the numerical calculations, the form as given in Eq. (5) is more suitable for the development of approximations to the exact numerical results, as shown below.

### III. RESULTS

All the numerical results to be discussed below are presented in effective GaAs units, corresponding to the following choice of material parameters:  $m_e^* = 0.067m_0$ ,  $m_h^* = 0.268m_0$ , and  $\epsilon = 12.5$ , with  $m_0$  being the bare-electron mass. The effective Bohr radius for the electron ( $a_0^*$ ) is then equal to 98.7 Å, and the associated effective Rydberg ( $\text{Ry}^*$ ) is equal to 5.83 meV. Values of  $eF$  are given in units of  $\text{Ry}^*/a_0^* \simeq 0.059 \text{ meV}/\text{Å}$ . Regarding the geometrical parameters defining the size of the double ring, we have chosen a configuration with  $R_e < R_h$ :  $R_e = 300 \text{ Å}$ ,  $R_h = 330 \text{ Å}$ . For this double-ring size, the parameter  $r$  in Eq. (3) equals 0.995. We know from Ref. [28] that in this case the  $F = 0$  ground-state exciton is a strongly bounded exciton, meaning essentially that the eigenvalue  $\varepsilon_{L,n}(B)$  in Eq. (9) becomes  $L$  and magnetic field independent.

We have identified three possible characteristic regimens for a radially polarized exciton, depending on the intensity of the applied in-plane electric field. They are shown schematically in Fig. 1, and termed the quasifree exciton (I), the locked exciton (II), and the broken exciton or electron-hole pair (III), for increasing electric field strength. The characteristic values of the electron and hole angular coordinates in each of the three configurations are also indicated in the bottom panel (right) of Fig. 1, and as resulting from the numerical calculations in Fig. 2. Figure 2(a), corresponding to a zero electric field and trapped magnetic flux, shows the signatures of a quasifree exciton:  $\theta_e \simeq \theta_h$  [for optimizing the Coulomb attractive term  $U_c(\Delta\theta)$  with  $\Delta\theta \simeq 0$ ], but all values for  $\theta_e \simeq \theta_h$  between 0 and  $2\pi$  occur with equal probability. By increasing the electric field, the probability associated with the locked configuration  $\theta_e \simeq \theta_h \simeq \pi$  increases its value [Figs. 2(b) and 2(c)], since the system tries now to optimize both the Coulomb attraction and the electrostatic energy. On further increase of the electric field, the system becomes partially quasifree and partially broken [Fig. 2(d)], and finally in the high-electric-field limit the system fully adopts the broken configuration, since in this limit the physics is dominated by the electrostatic contribution  $-eF(R_e + R_h)$  to the total energy of the system. The three regimens are displayed in Fig. 3, where the lowest-lying exciton energy levels are plotted as functions of the electric field, for  $\phi_{c.m.} = 0$ , and for a particular realization of the structured ring. The full lines correspond to the numerical (exact) results, while the dotted and dashed lines correspond to different approximations, to be explained below. Note that except for the ground state, the levels are organized in doublets, progressively split by increasing the electric field. At  $F = 0$ ,

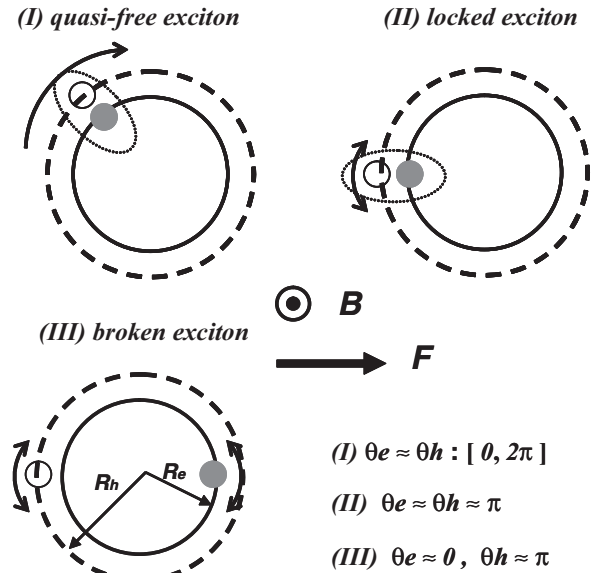


FIG. 1. Schematic view of the three possible regimens for the charge-tunable exciton; empty (filled) small circle represents the hole (electron). The strength of the applied electric field is such that  $F_I < F_{II} < F_{III}$ , at fixed values of  $B$ ,  $R_e$ , and  $R_h$ . The electric field  $F$  is along the positive direction of the  $x$  axis, the magnetic field  $B$  points along the positive direction of the  $z$  axis, and  $R_h > R_e$ .

the total angular quantum number  $L$  is well defined. In this way, the ground state belongs to the exciton which has  $L = 0$  at  $F = 0$ , the next doublet evolves from the  $L = \pm 1$  zero-electric-field exciton, and so on. Naturally, all doublets are degenerate at  $F = 0$ . The dashed line with a large slope, proportional to  $-eF(R_e + R_h)$ , essentially distinguishes the quasifree and locked configurations (region at the left of the high-slope

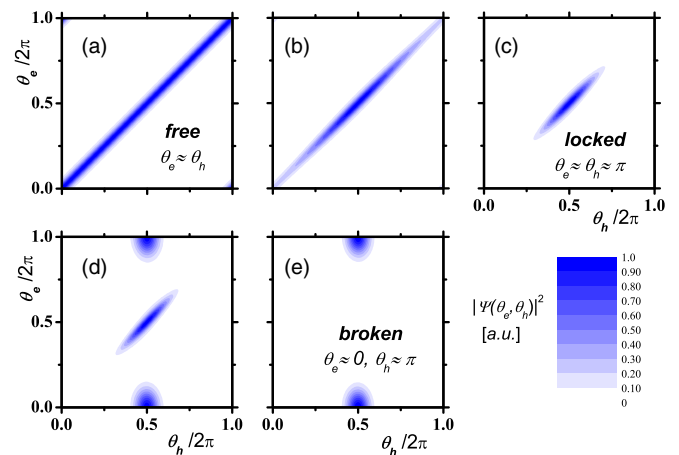


FIG. 2. (Color online) Exciton ground-state probability distribution  $|\varphi_0(\theta_e, \theta_h)|^2$  in the  $(\theta_e, \theta_h)$  domain. Values of  $eF$  are given in  $\text{Ry}^*/a_0^*$  effective units. (a)  $eF = 0$ ,  $\phi_{c.m.}/\phi_0 = 0$ ; (b)  $eF = 0.02$ ,  $\phi_{c.m.}/\phi_0 = 0$ ; (c)  $eF = 0.25$ ,  $\phi_{c.m.}/\phi_0 = 0.42$ ; (d)  $eF = 0.54$ ,  $\phi_{c.m.}/\phi_0 = 0.21$ ; (e)  $eF = 0.60$ ,  $\phi_{c.m.}/\phi_0 = 0.525$ . The three discussed regimens (a), (c), and (e) can be clearly seen, as well as the transition points (b) and (d). For cases (d) and (e), note that the configurations  $\theta_e \approx 0$ ,  $\theta_h \approx \pi$  and  $\theta_e \approx 2\pi$ ,  $\theta_h \approx \pi$  are equivalent, due to the ring geometry.

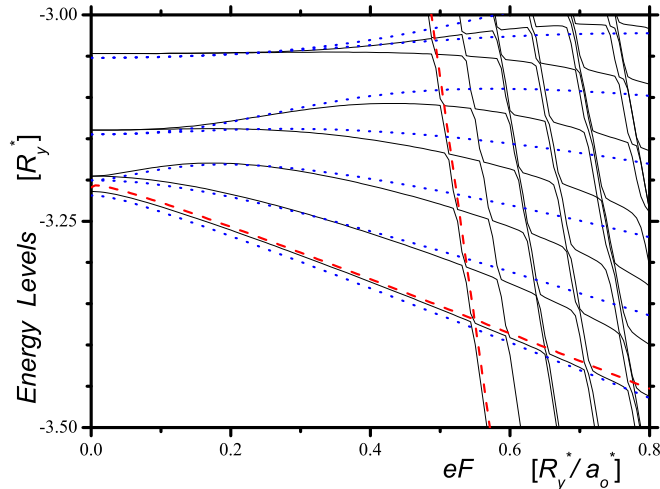


FIG. 3. (Color online) Lowest-lying exciton energy levels versus applied electric field, at  $\phi_{c.m.} = 0$  ( $B = 0$ );  $R_e = 300 \text{ \AA}$ ,  $R_h = 330 \text{ \AA}$ . Full lines correspond to the numerically exact results, dotted lines are the solutions of the quasiparticle approximation [Eq. (13)], and dashed lines correspond to the locked and broken approximations (see the text). The flat-level region corresponds to the quasifree exciton regime, the low-slope [ $\sim -eF(R_h - R_e)$ ] levels to the locked exciton states, and the high-slope [ $\sim -eF(R_e + R_h)$ ] ones to the broken exciton states. Note that the *exact* results (full lines) never cross among them; see Fig. 5(d) for an enhanced view of the avoided crossings.

dashed line) from the broken exciton regime (region at the right of the high-slope dashed line). In other words,  $\Delta\theta \sim 0$  in the left region, while  $\Delta\theta \sim \pi$  in the right region. In addition, in the left region, one can distinguish between excitonic levels moving approximately linearly with the electric field [slope  $\sim -eF(R_h - R_e)$ ], and others showing a weak dependence on  $F$ . As shown below, the former correspond to the locked exciton regime, the latter to the quasifree regime. We will discuss now the main physical features of each of them, guided by numerically (exact) results and accurate analytical approximations.

### A. Regime I, quasifree exciton

This is the weak-electric-field limit, where the contribution  $H_F(\theta_0, \Delta\theta)$  in Eq. (5) may be considered as a small perturbation to the other two. In this regime, the c.m. coordinate runs over all possible values between 0 and  $2\pi$ , while the relative coordinate  $\Delta\theta$  is restricted to taking small values (that is,  $|\Delta\theta| \ll 2\pi$ ), in order to optimize the electron-hole Coulomb attraction  $U_c(\Delta\theta)$  [32]. This suggests that in this regime one is allowed to take the  $\Delta\theta \rightarrow 0$  limit of Eq. (8), obtaining

$$H_F(\theta_0, \Delta\theta \rightarrow 0) \approx eF \left[ (R_h - R_e) \cos \theta_0 + \left( \frac{R_e I_h + R_h I_e}{I} \right) (\sin \theta_0) \Delta\theta + O(\Delta\theta^2) \right]. \quad (12)$$

At leading order in  $\Delta\theta$  ( $\Delta\theta^0$ ), an effective decoupling of the c.m. and relative coordinates is achieved, which allow us to approximate the full Hamiltonian in Eq. (5) by the following

quasiparticle (qp) one:

$$H_{exc}^{qp}(\theta_0, \Delta\theta) = H_{c.m.}^{qp}(\theta_0) + H_{int}(\Delta\theta), \quad (13)$$

with

$$H_{c.m.}^{qp}(\theta_0) = \frac{\hbar^2}{2I} \left( -i \frac{\partial}{\partial \theta_0} + \frac{\phi_{c.m.}}{\phi_0} \right)^2 + eF(R_h - R_e) \cos \theta_0, \quad (14)$$

and  $H_{int}(\Delta\theta)$  defined in Eq. (7). In the limit of vanishing or small electric field, Eq. (13) has the following analytical estimate:

$$E_{L,n}^1(B, F \rightarrow 0) = \frac{\hbar^2}{2I} \left( L + \frac{\phi_{c.m.}}{\phi_0} \right)^2 + \varepsilon_n, \quad (15)$$

with

$$\varepsilon_n = -\frac{e^2/\epsilon}{R_e + R_h} - \frac{\alpha^2 \hbar^2}{8I_{int}} \left[ 1 - 2n + \left( 1 + \frac{8I_{int} V_0}{\alpha^2 \hbar^2} \right)^{1/2} \right]^2. \quad (16)$$

Here,

$$V_0 = \frac{e^2}{\epsilon} \left( \frac{1}{|R_e - R_h|} - \frac{1}{R_e + R_h} \right) > 0, \quad (17)$$

and  $\alpha = 5.458$ ,  $n = 1, 2, \dots$  [28]. Equation (15) is an approximation to Eq. (9), valid in the limit where the exciton is strongly bounded, meaning that the “binding energy”  $\varepsilon_{L,n}(B)$  is essentially independent of  $L$  and  $B$ . The approximation amounts to replacing  $\varepsilon_{L,n}(B)$  by  $\varepsilon_n$ , with the corresponding expression for the latter in Eq. (16) being derived in the Appendix of Ref. [28] (see [33]). In this regime, the negative of the binding energy in Eq. (15) is much greater than the first term, related to the kinetic energy of the c.m. motion. Evaluating for  $\phi_{c.m.} = 0$  and  $n = 1$ , we obtain  $E_{0,1}^1 \simeq -3.21Ry^*$ ,  $E_{\pm 1,1}^1 \simeq -3.19Ry^*$ ,  $E_{\pm 2,1}^1 \simeq -3.14Ry^*$ , and  $E_{\pm 3,1}^1 \simeq -3.043Ry^*$ , in excellent agreement with the numerically exact values (full lines) displayed in Fig. 3, in the limit of small electric field.

The effective c.m. Hamiltonian  $H_{c.m.}^{qp}(\theta_0)$  may in turn be expressed in the following suggestive way:

$$H_{c.m.}^{qp}(\theta_0) = \frac{\hbar^2}{2I} \left( i \frac{\partial}{\partial \theta_0} + \frac{\phi_{c.m.}^*}{\phi_0^*} \right)^2 + e^* F R^* \cos \theta_0, \quad (18)$$

where  $e^* = e(R_h - R_e)/(R_h + R_e)$ ,  $R^* = R_h + R_e$ ,  $\phi_0^* = ch/e^*$ , and  $\phi_{c.m.}^* = \pi B R^{*2}$ . Accordingly,  $H_{c.m.}^{qp}(\theta_0)$  can be considered as corresponding to a quasiparticle of *effective* electrical charge  $e^*$ , orbiting in a ring of *effective* radius  $R^*$ . The size, and even the sign, of the charge  $e^*$  may be changed at will by changing the geometrical parameters  $R_h$  and  $R_e$ . The solutions of  $H_{exc}^{qp}(\theta_0, \Delta\theta)$  are the dotted lines of Fig. 3. As expected, they are a good approximation to the exact results in the bounded exciton region, but fails in the broken or electron-pair region, where the assumption of a bound exciton with  $\Delta\theta \sim 0$  is not valid. Actually, the (approximate) point of departure between the exact and approximate solutions signals the qualitative breakdown of the small-oscillation assumption for  $\Delta\theta$ .

### B. Regime II, locked exciton

This regime is characterized by the fact that the bounded exciton ( $\Delta\theta \simeq 0$ ) becomes essentially localized around

$\theta_0 \simeq \pi$ . The electric field is strong enough to localize the c.m. degree of freedom, losing some kinetic energy but gaining the dipolar electrostatic energy of the bounded exciton, of the order of  $-eF(R_h - R_e)$  (see below). Expanding Eq. (14) around  $\theta_0 \simeq \pi$  we obtain

$$H_{\text{c.m.}}^{\text{II}}(\bar{\theta}_0) = -eF(R_h - R_e) + \frac{\hbar^2 \phi_{\text{c.m.}}^2}{2I \phi_0^2} - \frac{i\hbar^2 \phi_{\text{c.m.}}}{I \phi_0} \frac{\partial}{\partial \bar{\theta}_0} - \frac{\hbar^2}{2I} \frac{\partial^2}{\partial \bar{\theta}_0^2} + \frac{eF(R_h - R_e)}{2} \bar{\theta}_0^2, \quad (19)$$

with  $\bar{\theta}_0 = \theta_0 - \pi$ . Considering that the first two terms on the right-hand side (RHS) of the equation above are just constants and that the last two in the second line define an effective one-dimensional harmonic oscillator for the dynamics of the c.m. motion, one obtains an approximate expression for the eigenvalues for this regime as

$$E_{m,n}^{\text{II}}(B, F) \simeq -eF(R_h - R_e) + \frac{\hbar^2 \phi_{\text{c.m.}}^2}{2I \phi_0^2} + \hbar\omega_{eh} \left( m + \frac{1}{2} \right) + \varepsilon_n \quad (20)$$

with  $\omega_{eh} = \sqrt{eF(R_h - R_e)/I}$ , and  $\varepsilon_n (< 0)$  is the same exciton ‘‘binding energy’’ as in Eq. (15). The assumption behind this analytical estimate is that in this regime the exciton, although localized, still is strongly bounded. Within this harmonic approximation for the c.m. motion, the contribution from the third term in Eq. (19) (linear in  $\phi_{\text{c.m.}}$ ) is just zero if evaluated in a perturbative way, since it corresponds to the matrix element of different parity states. The low-slope dashed line in Fig. 3 corresponds to the approximation in Eq. (20) for the energy of the ground-state exciton ( $m = 0, n = 1$ ) in the locked regime. Excited exciton energies may be obtained from Eq. (20) for increasing values of  $m$ , keeping  $n$  fixed at its lowest value  $n = 1$ . This results in a set of low-slope lines (not shown), that follows closely the quasiparticle dashed lines. By taking the difference  $E_{m+1,n}^{\text{II}}(B, F) - E_{m,n}^{\text{II}}(B, F) = \hbar\omega_{eh}$ , one obtains that  $\hbar\omega_{eh}/Ry^* \simeq 0.07$  for  $eF/(Ry^*/a_0^*) = 0.4$ , in good agreement with the spacing between two consecutive exciton energy levels in Fig. 3, for this particular value of the electric field.

For  $R_e > R_h$ , the equilibrium position of the locked exciton is around  $\theta_e \simeq \theta_h \simeq \theta_0 \simeq 0$ ; the same results are obtained by expanding now about  $\theta_0 \simeq 0$ , but with the  $e \leftrightarrow h$  change.

### C. Regime III, broken exciton

In this regime, roughly expected for  $eF(R_h + R_e) > -\varepsilon_1$ , the hole is locked around  $\theta_h \simeq \pi$  and the electron at  $\theta_e \simeq 0$ . The electric field is strong enough to disrupt the bound exciton. For the approximate analysis of this regime, it is convenient to start from Eq. (1), rewritten as

$$H_{\text{exc}}(\theta_e, \theta_h) = H_e(\theta_e) + H_h(\theta_h) + U_c(\Delta\theta), \quad (21)$$

with

$$H_x(\theta_x) = \frac{\hbar^2}{2I_x} \left( -i \frac{\partial}{\partial \theta_x} + \eta_x \frac{\phi_x}{\phi_0} \right)^2 - q_x F R_x \cos \theta_x, \quad (22)$$

with  $q_e = e, q_h = -e$  and  $\eta_e = +1, \eta_h = -1$ . In the broken exciton regime, both Hamiltonians  $H_e(\theta_e)$  and  $H_h(\theta_h)$  may be expanded around their respective equilibrium positions. For instance,

$$H_e^{\text{III}}(\theta_e) = -eFR_e + \frac{\hbar^2 \phi_e^2}{2I_e \phi_0^2} - \frac{i\hbar^2 \phi_e}{I_e \phi_0} \frac{\partial}{\partial \theta_e} - \frac{\hbar^2}{2I_e} \frac{\partial^2}{\partial \theta_e^2} + \frac{eFR_e}{2} \theta_e^2. \quad (23)$$

Since this Hamiltonian (and the one associated with the hole) is quite similar to the one in Eq. (19), one can proceed in a similar manner, obtaining the following approximate expression for the energy of the broken exciton:

$$E_{n_e, n_h}^{\text{III}}(B, F) \simeq -eFR^* + \hbar\omega_e \left( \frac{1}{2} + n_e \right) + \hbar\omega_h \left( \frac{1}{2} + n_h \right) + \frac{\hbar^2 \phi_e^2}{2I_e \phi_0^2} + \frac{\hbar^2 \phi_h^2}{2I_h \phi_0^2} + U_c(\pi), \quad (24)$$

where  $\omega_x = \sqrt{eFR_x/I_x}$ , and  $U_c(\pi) = -e^2/(\epsilon R^*)$  is the residual  $e$ - $h$  Coulomb interaction. The high-slope dashed line in Fig. 3 corresponds to the approximation in Eq. (24) for the energy of the ground-state exciton ( $n_e = n_h = 0$ ) in the broken regime. Clearly, excited energy states in this regime may be obtained by allowing higher values for  $n_e$  and  $n_h$ ; this will result in a set of high-slope lines (not shown). For the polarized ring considered here,  $\omega_e/\omega_h \simeq 2$ , and accordingly more ‘‘holelike’’ modes will be occupied than ‘‘electronlike’’ modes ( $n_e \leq n_h$ ). From the condition  $eF(R_h + R_e) \sim -\varepsilon_1$ , one obtains an estimate of the strength of the electric field needed to disrupt the bounded exciton: taking  $\varepsilon_1 \simeq E_{0,1}^1 \simeq -3.21Ry^*$ , one obtains that  $eF/(Ry^*/a_0^*) \sim 0.5$  for this threshold electric field, once again in good agreement with the results in Fig. 3.

### D. Discussion

We show in Fig. 4 the excitonic energy levels as the trapped flux  $\phi_{\text{c.m.}}$  changes, for increasing values of the electric field. Figure 4(a) corresponds to the zero-electric-field situation; in this case, the exciton energy levels are given by Eq. (9). All levels plotted in Fig. 4(a) belong to the  $n = 0$  exciton, and for  $L = 0, \pm 1, \pm 2, \pm 3$ . Having different (well-defined) quantum numbers, the energy levels cross at each intersection. The optical activity of the  $L = 0$  state is denoted by the shadowed area about it [34]. To characterize the excitonic states as bright (optically active) or dark (optically inert), we evaluate the oscillator strength (OS), i.e., the angular overlap of the electron and the hole in a given exciton eigenstate [35],

$$S_i \propto \left| \int_0^{2\pi} d\theta \varphi_i(\theta_e = \theta, \theta_h = \theta) \right|^2. \quad (25)$$

Note that, in our chosen zero-electric-field basis of Eq. (10), only states with  $l_e + l_h = 0$  contribute to the OS. Thus, at zero transverse electric field  $F$ , only the  $L = 0$  exciton is bright. At finite values of  $F$  the azimuthal symmetry of the system is broken, and  $L$  is no longer a good quantum number. The new exciton eigenfunctions can be considered as a mixing of

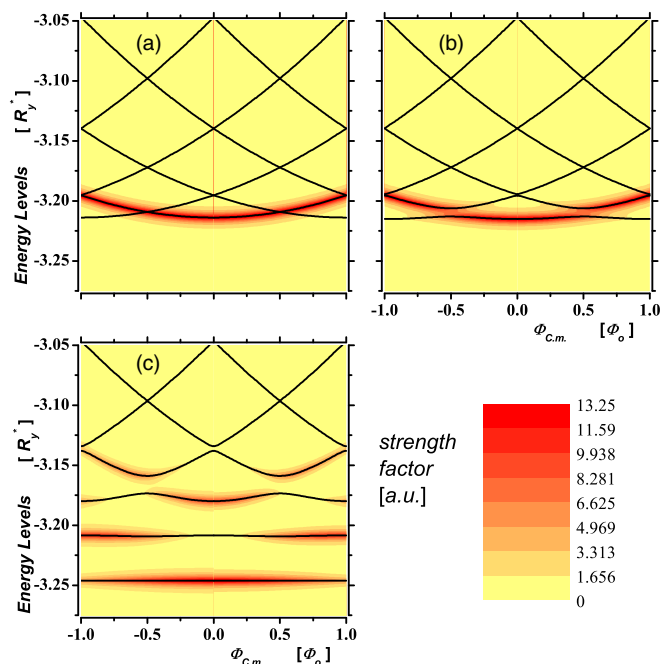


FIG. 4. (Color online) Exciton energy levels vs trapped magnetic flux, at fixed values of  $eF$ . The spectra are approximately periodic in the trapped flux; this is not a property of the full system but of the bounded excitonic states. (a)  $eF = 0$ ; only the  $L = 0$  exciton is optically active. (b)  $eF = 0.02Ry^*/a_0^*$ ; the crossing levels become anticrossings, and this property allows for the experimental manipulation of the exciton state. (c)  $eF = 0.15Ry^*/a_0^*$ ; the low-energy flat (i.e., flux-independent) levels correspond to locked exciton states, and optical activity appears in many of them, depending on the precise value of  $\phi_{c.m.}$ , allowing also for resonant induced transitions between them.

the old ones, and then the projection of them on the old  $L = 0$  eigenfunction gives their OS [34]. A multiplicative factor must be included (in principle) in the definition of the OS in Eq. (25), to account for the finite *radial* overlap of the electron and hole wave functions, which we have not considered explicitly in this work. A detailed analysis of this issue for a possible realization of  $e$ - $h$  quantum rings in volcanolike InGaAs heterostructures has been performed in Ref. [36].

Figures 4(b) and 4(c) correspond to increasing values of the electric field: the system loses the azimuthal symmetry along the  $z$  axis and the pair  $(L, n)$  is replaced by a single quantum number. Levels now repel each other, and a gap appears at each crossing of the  $F = 0$  case. Gaps are barely discernible in Fig. 4(b) (except for the lowest one at  $\phi_{c.m.} = \pm 0.5\phi_0$ ), but they are quite prominent in Fig. 4(c). The reason why the electric field is much less effective in opening gaps at crossing points at higher energies is quite simple: considering that the electric field acts as a perturbation on the zero-field eigenstates, one finds that it mixes only zero-field eigenstates with  $L$ 's differing by unity (that is,  $L$  with  $L \pm 1$ ). Then, for example, the gap at  $\phi_{c.m.} = +(-)0.5\phi_0$  appears at the crossing of the  $L = 0$  and  $L = -1 (+1)$  parabolas, which are directly mixed by the electric field, resulting in a gap linear in the electric field. All other gaps in the displayed spectra are of higher order in

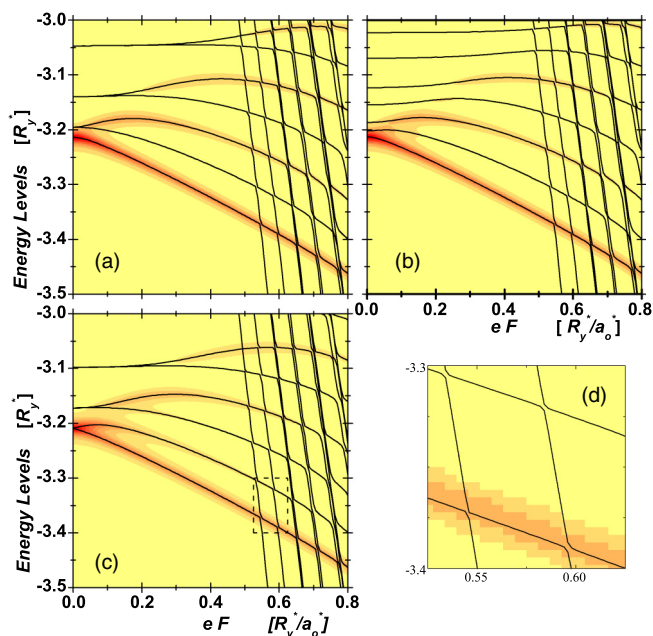


FIG. 5. (Color online) Exciton energy levels versus applied electric field, at fixed values of the center-of-mass trapped flux  $\phi_{c.m.}$ : (a)  $\phi_{c.m.} = 0$ ; (b)  $\phi_{c.m.} \simeq 0.21\phi_0$ ; (c)  $\phi_{c.m.} = 0.5\phi_0$ .  $R_e = 300 \text{ \AA}$ ,  $R_h = 330 \text{ \AA}$ . Color scale for the strength factor as in Fig. 4. (d), showing the avoided crossings, corresponds to an enhanced view of the rectangular sector in (c) enclosed by straight dashed lines.

$F$ , since they correspond to crossing of parabolas differing by more than unity in their  $L$  values. Under the assumption of weak electric fields, higher orders in  $F$  are equivalent to smaller gaps. Note that the assumption of weak electric field may be made *always* valid, by moving to higher energies in the excitonic spectra.

Figure 5 displays how the excitonic energy levels depend on the applied electric field, for different values of  $\phi_{c.m.}$ . Figure 5(c), corresponding to  $\phi_{c.m.} = 0.5\phi_0$ , exhibits a different organization in doublets, as compared with the  $\phi_{c.m.} = 0$  case. In particular, the ground-state doublet corresponds to the  $L = 0, -1$  zero-electric-field states, which are directly mixed by it, resulting in an anticrossing gap which opens linearly in  $eF$ . In Fig. 5(d) we provide an enhanced view of a few anticrossing points of the exciton energy spectrum, making clear the point that as soon as  $F \neq 0$ , all the degeneracies present at the intersecting parabolas in Fig. 4(a) are strictly removed, and then the energy levels in Fig. 5 (as in Fig. 3) never cross among them, as stated above. Another interesting point to be addressed here is the fact that if one follows adiabatically the first excited exciton energy level, for increasing values of the electric field it passes through the following sequence of configurations: quasifree  $\rightarrow$  locked ( $m = 1, n = 1$ )  $\rightarrow$  broken ( $n_e = n_h = 0$ )  $\rightarrow$  locked ( $m = 0, n = 1$ )  $\rightarrow$  broken ( $n_e = 0, n_h = 1$ ). For the ground-state exciton, the only possible sequence is quasifree  $\rightarrow$  locked ( $m = 0, n = 1$ )  $\rightarrow$  broken ( $n_e = n_h = 0$ ), but for higher excited excitons several changes of configurations are possible, starting always from the quasifree one, and jumping then back and forth between the locked and broken configurations. Noting that the locked  $m = 0, n = 1$

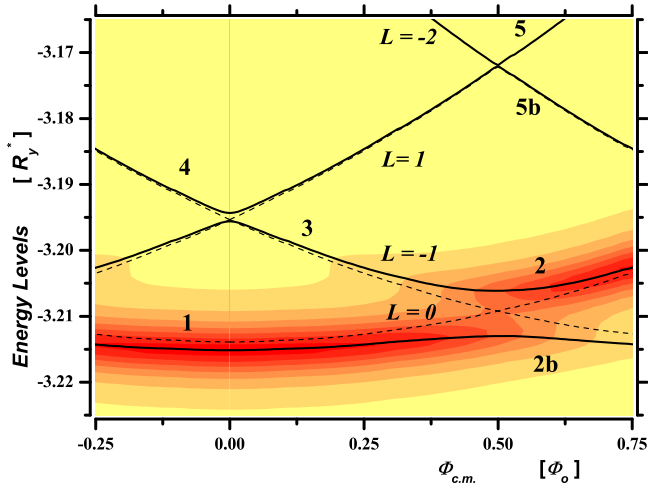


FIG. 6. (Color online) Schematic view in  $E_i, \phi_{c.m.}$  space of the suggested protocols for the dynamical storage of photoinduced excitons. Dashed lines correspond to exciton energies for  $eF = 0$ ,  $E_{L,n}(B)$ , while full lines are for  $eF = 0.05Ry^*/a_0^*$ ,  $E_i(B, F)$ . The labels  $L = 0, \pm 1, \pm 2$ , are associated with the zero-field exciton levels. The shaded regions correspond to the bright states. Using the electric field as a switch, i.e., converting crossing points to anticrossing ones, the exciton can navigate the Hilbert space [38]. Possible storage protocols are described in the text.

ground-state configuration is always bright, this provides a possible way to manipulate excitons, converting them from dark to bright by application of suitable (strong) electric fields. We suggest in what follows another manipulation strategy, based on the application of smaller electric fields (i.e., without breaking the exciton).

It seems quite possible that the main application of these systems will be related to the feasibility of storing excitons, in either isolated ring configurations or ring ensembles. This storage is achieved by switching the ring ensemble from an optically active state (bright) to an optically passive one (dark). Simple mechanisms involving magnetic or electrical fields have been previously proposed. One such mechanism is suggested in Ref. [37]. It involves the use of an in-plane electric field for a single-radius ( $R_e = R_h$ ) ring. Their dark situation corresponds to the destruction of the exciton, with the electron and the hole localized in opposite sides of the ring (our broken exciton regimen III). In fact, as the authors of Ref. [37] discuss, the critical electrical field strength is comparable to the electron-hole interaction strength, i.e., our exciton rupture field, given by the equation  $eF(R_e + R_h) \sim -\varepsilon_1$ . The internal structure of the rings analyzed in this article (variable  $R_e$  and  $R_h$ ), which generates a non-neutral exciton, allows it to be manipulated via both electric and magnetic fields without destroying the exciton. In Fig. 6 we show the exciton spectra both for zero electric field (broken lines) and with a small field ( $eF = 0.05Ry^*/a_0^*$ ). The shaded regions correspond to the bright exciton states. A protocol to store the exciton without breaking it can be easily designed, using the fact that the electric field changes the crossing points of the spectra into anticrossing ones. A tentative protocol might be as follows. Step 1: at  $eF = 0$ ,  $\phi_{c.m.}$  is increased from 0 to above  $0.5\phi_0$ ,

i.e., the exciton is moved (see Fig. 6) from point 1 to point 2. Step 2: the electric field is switched on, converting the crossing point at  $\phi_{c.m.} = 0.5\phi_0$  into an anticrossing one. Step 3:  $\phi_{c.m.}$  is decreased towards zero, moving the exciton from point 2 to point 3, a dark state. The protocol above assumes an adiabatic movement of the exciton, i.e., a slow rate of variation of the fields. It is also possible to maintain a fixed electric field, and use a *diabatic* evolution to arrive at point 2, and then an adiabatic one to move the system to point 3.

A cyclic protocol, suitable for an array of radially polarized rings [27], is also possible, as follows. Step 1:  $\phi_{c.m.}$  is increased from  $-0.05\phi_0$  to  $0.55\phi_0$ , with a small electric field applied. The ground-state exciton, if present (i.e., photoexcited), moves from point 1 to point 2b in Fig. 6 following the full line. Step 2: the electric field is turned off and  $\phi_{c.m.}$  is reversed to  $-0.05\phi_0$ . Repeat cyclically. If after step 1 the exciton was at 2b, after step 2 it will move from 2b to 4, following now the dashed line. Once there, in the first step of the next cycle it will move from 4 to 5b, and so on. The net result is that the exciton becomes trapped in the high-energy region of the available spectra, and is essentially dark. If a ring of the ensemble fails to catch an exciton, or if it decays before arriving at point 2b, the ring is ready to catch one in the next cycle. In this way, under photoexcitation, each ring of the array will be filled with one exciton, albeit stored in different levels of the spectra. In practice, the “climbing” movement of the exciton along the energy spectra has a limit, since the gaps at the anticrossing points become increasingly small for ascending energies, and the switching strategy fails. For example, in going from point 4 to point 5b, if the gap is small, the exciton may follow with some probability a diabatic trajectory and arrive instead at point 5. Once the exciton is on the wrong track, the same cycles move it back to point 1, where it is optically active again. Therefore, this cyclic protocol can be used to introduce a tunable delay in the incoming photons.

Some conditions must be fulfilled for this protocol to be realized in practice. For example, the temperature should be such that at least the two first gaps at  $\phi_{c.m.} = 0, 0.5\phi_0$  should be larger than  $k_B T$ . Considering that the gap at  $\phi_{c.m.} = 0$  is about  $10^{-3}Ry^* = 5.83 \times 10^{-3}$  meV, this results in the constraint  $T \lesssim 0.05$  K [39]. Since this temperature is much smaller than the Debye temperature of GaAs ( $\sim 345$  K) [40], one can expect that exciton decay via interactions with the phonon bath will be small. Also, the electric field strength in Fig. 6 is about 300 V/cm, much smaller than the fields formed at the depletion layer of *n-p* semiconductor junctions ( $\sim 10^3$ – $10^5$  V/cm).

#### IV. CONCLUSIONS

We have studied theoretically the excitonic spectrum of radially polarized semiconductor nanorings, in the presence of an in-plane uniform electric field and a perpendicular magnetic field. Based on the numerically exact solution, we have identified three different regimens for the exciton, for increasing values of the electric field: (a) quasifree excitons; (b) locked excitons; and (c) electron-hole pairs or broken excitons. Accurate analytical approximations are provided for each one of the three regimens. In the first regime, corresponding to weak electric fields, the exciton behaves

as a single charged particle, with an effective electric charge determined by the nanoring geometrical parameters. Protocols are suggested for the dynamical storage of excitons *without destroying them*, by a combination of magnetic and electric fields, and by following a sequence of well-defined steps. This may have some impact in the context of trapping light for later use.

## ACKNOWLEDGMENTS

M.P. would like to acknowledge financial support from FONDECYT under Grant No. 1100672 and from DGIP/USM under Grant No. 11.11.62. J.S. and C.R.P. acknowledge partial financial support from CONICET(Argentina) as Fellows and under Grant No. PIP 02753/00.

- 
- [1] Y. Aharonov and D. Bohm, *Phys. Rev.* **115**, 485 (1959).
- [2] V. Chandrasekhar, R. A. Webb, M. J. Brady, M. B. Ketchen, W. J. Gallagher, and A. Kleinsasser, *Phys. Rev. Lett.* **67**, 3578 (1991).
- [3] D. Mailly, C. Chapelier, and A. Benoit, *Phys. Rev. Lett.* **70**, 2020 (1993).
- [4] U. Keyser, S. Borck, R. Haug, M. Bichler, G. Abstreiter, and W. Wegscheider, *Semicond. Sci. Technol.* **17**, L22 (2002).
- [5] A. Tonomura, N. Osakabe, T. Matsuda, T. Kawasaki, J. Endo, S. Yano, and H. Yamada, *Phys. Rev. Lett.* **56**, 792 (1986).
- [6] B. C. Lee, O. Voskoboynikov, and C. P. Lee, *Physica E* **24**, 87 (2004).
- [7] M. Bayer, M. Korkusinski, P. Hawrylak, T. Gutbrod, M. Michel, and A. Forchel, *Phys. Rev. Lett.* **90**, 186801 (2003).
- [8] J. Cui, Q. He, X. M. Jiang, Y. L. Fan, X. J. Yang, F. Xue, and Z. M. Jiang, *Appl. Phys. Lett.* **83**, 2907 (2003).
- [9] A. Lorke, R. J. Luyken, A. O. Govorov, J. P. Kotthaus, J. M. Garcia, and P. M. Petroff, *Phys. Rev. Lett.* **84**, 2223 (2000).
- [10] V. Halonen, P. Pietilainem, and T. Chakraborty, *Europhys. Lett.* **33**, 377 (1996).
- [11] Z. Barticevic, M. Pacheco, and A. Latgé, *Phys. Rev. B* **62**, 6963 (2000).
- [12] A. Bruno-Alfonso and A. Latgé, *Phys. Rev. B* **61**, 15887 (2000).
- [13] Y. Li, H.-M. Lu, O. Voskoboynikov, C. P. Lee, and S. M. Sze, *Surf. Sci.* **532-535**, 811 (2003).
- [14] Z. Barticevic, G. Fuster, and M. Pacheco, *Phys. Rev. B* **65**, 193307 (2002).
- [15] R. J. Warburton, C. Schaflein, D. Haft, F. Bickel, A. Lorke, K. Karrai, J. Garcia, W. Schoenfeld, and P. Petroff, *Physica E* **9**, 124 (2001).
- [16] D. Haft, C. Schulhauser, A. Govorov, R. Warburton, K. Karrai, J. Garcia, W. Schoenfeld, and P. Petroff, *Physica E* **13**, 165 (2002).
- [17] E. Ribeiro, A. O. Govorov, W. Carvalho, and G. Medeiros-Ribeiro, *Phys. Rev. Lett.* **92**, 126402 (2004).
- [18] H. Hu, J. L. Zhu, D. J. Li, and J. J. Xiong, *Phys. Rev. B* **63**, 195307 (2001).
- [19] J. Song and S. E. Ulloa, *Phys. Rev. B* **63**, 125302 (2001).
- [20] J. I. Climente, J. Planelles, and W. Jaskolski, *Phys. Rev. B* **68**, 075307 (2003).
- [21] R. A. Romer and M. E. Raikh, *Phys. Rev. B* **62**, 7045 (2000).
- [22] S. Ulloa, A. Govorov, A. Kalameitsev, R. Warbuton, and K. Karrai, *Physica E* **12**, 790 (2002).
- [23] A. O. Govorov, S. E. Ulloa, K. Karrai, and R. J. Warburton, *Phys. Rev. B* **66**, 081309 (2002).
- [24] L. G. G. V. Diasda Silva, S. E. Ulloa, and A. O. Govorov, *Phys. Rev. B* **70**, 155318 (2004).
- [25] L. G. G. V. Diasda Silva, S. E. Ulloa, and T. V. Shahbazyan, *Phys. Rev. B* **72**, 125327 (2005).
- [26] A. V. Maslov and D. S. Citrin, *Phys. Rev. B* **67**, 121304 (2003).
- [27] T. Mano, T. Kuroda, S. Sanguinetti, T. Ochiai, T. Tateno, J. Kim, T. Noda, M. Kawabe, K. Sakoda, G. Kido, and N. Koguchi, *Nano Lett.* **5**, 425 (2005).
- [28] Z. Barticevic, M. Pacheco, J. Simonin, and C. R. Proetto, *Phys. Rev. B* **73**, 165311 (2006).
- [29] The characterization of the zero-electric-field exciton as extended or localized refers to the degree of localization of the exciton wave function in the relative-angle coordinate. In both cases, the center-of-mass coordinate rotates freely around the ring.
- [30] L. Jacak, P. Hawrylak, and A. Wójs, *Quantum Dots* (Springer, Berlin, 1997).
- [31] V. V. Arsooski, M. Z. Tadic, and F. M. Peeters, *Phys. Rev. B* **87**, 085314 (2013).
- [32] For a plot of  $U_c(\Delta\theta)$  vs  $\Delta\theta$  for this particular type of ring, see Fig. 4 in Ref. [28]. The limit  $|\Delta\theta| \ll 2\pi$  was characterized as the strongly interacting (SI) regime there. In the present context, both regime I and regime II are in this SI regime.
- [33] Equations (A1) and (A2) in the Appendix of Ref. [28] should be corrected as follows. In Eq. (A1), in the first term on the RHS, the denominator  $|R_e - R_b|$  should be replaced by  $R_e + R_b$ , while in the second term  $\cosh(\alpha\Delta\theta)$  must be replaced by  $\cosh^2(\alpha\Delta\theta)$ . Concerning Eq. (A2), it must be corrected as in Eq. (16).
- [34] In order to plot the OS in the figures, we use the equation  $S(E) = \sum_i S_i \delta(E - E_i) \approx \sum_i S_i \eta^2 / [(E - E_i)^2 + \eta^2]$ , with  $\eta$  being a small number, and  $i$  running over the exciton eigenstates.
- [35] M. D. Teodoro, V. L. Campo, V. Lopez-Richard, E. Marega, G. E. Marques, Y. G. Gobato, F. Iikawa, M. J. S. P. Brasil, Z. Y. AbuWaar, V. G. Dorogan, Y. I. Mazur, M. Benamara, and G. J. Salamo, *Phys. Rev. Lett.* **104**, 086401 (2010).
- [36] B. Li and F. M. Peeters, *Phys. Rev. B* **83**, 115448 (2011).
- [37] A. M. Fischer, V. L. Campo, M. E. Portnoi, and R. A. Romer, *Phys. Rev. Lett.* **102**, 096405 (2009).
- [38] G. E. Murgida, D. A. Wisniacki, and P. I. Tamborenea, *Phys. Rev. B* **79**, 035326 (2009).
- [39] This constraint on the temperature can be relaxed easily by about one order of magnitude, by the simple procedure of increasing slightly the electric field strength. Note for example how the barely discernible gap at  $\phi_{c.m.} = 0$  at  $eF/(Ry^*/a_0^*) = 0.02$  in Fig. 4(b) becomes a sizable gap ( $\sim 4$  K) for  $eF/(Ry^*/a_0^*) = 0.15$  in Fig. 4(c).
- [40] J. C. Holste, *Phys. Rev. B* **6**, 2495 (1972).